LAWRENCE
LIVERMORE
NATIONAL
LABORATORY

UCRL-JRNL-209079

Shock Initiation of Energetic Materials at Different Initial Temperatures

P. A. Urtiew, C. M. Tarver

January 19, 2005

Combustion, Explosions, and Shock Waves

Shock Initiation of Energetic Materials at Different Initial Temperatures

Paul A. Urtiew and Craig M. Tarver
Energetic Materials Center
Lawrence Livermore National Laboratory
Livermore, CA 94551 U. S. A.

Abstract

Shock initiation is one of the most important properties of energetic materials, which must transition to detonation exactly as intended when intentionally shocked and not detonate when accidentally shocked. The development of manganin pressure gauges that are placed inside the explosive charge and record the buildup of pressure upon shock impact has greatly increased the knowledge of these reactive flows. This experimental data, together with similar data from electromagnetic particle velocity gauges, has allowed us to formulate the Ignition and Growth model of shock initiation and detonation in hydrodynamic computer codes for predictions of shock initiation scenarios that cannot be tested experimentally. An important problem in shock initiation of solid explosives is the change in sensitivity that occurs upon heating (or cooling). Experimental manganin pressure gauge records and the corresponding Ignition and Growth model calculations are presented for two solid explosives, LX-17 (92.5 % triaminotrinitrobenzene (TATB) with 7.5 % Kel-F binder) and LX-04 (85 % octahydro-1,3,5,7-tetranitro-1,3,5,7-tetrazine (HMX) with 15 % Viton binder) at several initial temperatures.

Introduction

Energetic materials (EM) are widely used in both industrial applications and defense oriented establishments. Initiation of such materials is of particular interest for reason of safety as well as for control of the desired effect during their application. Energetic materials exist in gaseous state as well as condensed phase in homogeneous form, such as liquids and pastes, and in heterogeneous form, such as solid compositions consisting of granular mixtures of energetic materials with either energetic or inert binders.

There are various possible ways to initiate energetic materials. Gaseous mixtures, such as hydrogen and oxygen (H_2 and O_2), can easily be initiated with a spark, a heating element or an open flame. Condensed EM can be initiated by either mechanical or thermal heating or by any other kind of dynamic loading such as shock loading. Of all the initiation mechanisms, shock loading lends itself to the best quantitative analysis of the phenomenon, because it provides not only the measurable pressure and temperature to which the material is exposed but also provides accurate time duration of this exposure. Also important is the initial temperature of the material at which such dynamic loading

takes place, because increased temperature enhances the ability of material to chemically decompose leading to an increase of the material's shock sensitivity.

Therefore, the emphasis of this communication will be on shock initiation of energetic materials, predominantly heterogeneous solids, at different initial temperatures leading to the desired estimate of material sensitivity to dynamic loading.

Background

Initiation of gaseous mixtures and their eventual transition to detonation has been studied extensively in the early forties through sixties. An extensive review of these studies was written by Lee (1), which included a long list of references. Of interest here is the mechanism, which promotes initiation after shock loading and the mechanism of the transition to detonation. When a gaseous mixture is dynamically loaded, it becomes subject to auto ignition after a certain induction time, which is characteristic for that particular mixture. Once the mixture is ignited it burns releasing energy and enhancing the original shock wave. The flame, which may initially be laminar, becomes turbulent increasing the flame surface area and thus enhancing the shock wave even further. This process finally reaches the state where characteristic induction time for the pressure and temperature behind the enhanced shock wave become very small so that any additional kick, such as explosion of small pocket of trapped unburned mixture in the turbulent flame, may generate a strong detonation wave behind the initial shock wave. This overdriven wave then overcomes the original shock wave and propagates into the undisturbed mixture decaying to the self-sustaining detonation wave, which is characteristic for that particular mixture. This process is illustrated in Fig. 1.

Homogeneous liquid energetic materials behave very much in a similar fashion as the gaseous mixtures, except they require a much stronger shock wave to initiate the reaction and their induction times may be much shorter. Initiation of homogeneous liquid EM was recently reviewed by Dremin (2), who listed most of the pertinent references on the subject.

Initiation in a solid heterogeneous material takes place at the shock front itself accelerating it to the point where the transition to detonation takes place. The mechanism for the reaction at the wave front is attributed to the formation of the "hot spots", which appear at the voids and at interfaces between the granules of the material (3). These "hot spots" promote further reaction in their neighborhood increasing the burning area and creating a pressure pulse behind the shock wave. The transition to detonation occurs when this pressure pulse overtakes the leading shock front causing the shock pressure to rapidly increase and a detonation wave to form. This process will be described in more detail in the following sections.

Experimental Technique

Most of the experiments on solid heterogeneous materials in our laboratory were performed on the 100 mm bore, propellant driven gas gun, which allows close control of

the projectile velocity and of the loading pressure imposed on the EM target. The experimental set-up is illustrated in Fig 2.

The target assembly consisted of several discs of different thickness. Gauge packages containing manganin pressure gauges were embedded between individual discs. The gauges were armed with thin (125 μm) Teflon insulators on both sides to prevent shorting of the gauges in a conductive medium when the material becomes reactive. Other details of the manganin pressure gauges were described in our previous publications (4-9). For better control of the impact pressure a thin buffer plate of the same material as the impact plate is placed in front of the target assembly for symmetrical impact.

Also included in the target assembly are six tilt pins placed around the periphery of the target flush with the impact surface to measure tilt of the impact plate as it strikes the target, and two velocity pins sticking out some known distance from the target to measure velocity of the impact plate just before it strikes the target.

During the heated experiments nichrome foil spiral heaters were placed on both sides of the target separated by a thin aluminum disc for better heat distribution into the material under study. In this case gauge packages also contained thermocouples (TC) for better monitoring of the target temperature distribution during the heating cycle. The heating rate of the target was usually held constant initially at 3˚C/min until about10˚C below the desired temperature. Then it was changed to 1˚C/min until the final desired temperature is reached where it was held as long as necessary before the gun was fired.

Experimental Records

Following are the type of records obtained during the experimental phase of the initiation study of heterogeneous high explosives. Figures 3 and 4 show pressure records of shock loaded TATB-based insensitive high explosive LX-17, containing 92.5 weight % TATB and 7.5 weight % Kel-F binder pressed to 98.5 of theoretical maximum density initially at room temperature and at 250˚ C respectively.

The ambient LX-17, shown in Fig. 3, was shock loaded with an aluminum impactor flying at a velocity of 1.88 mm/μs, imposing a pressure of 11.0 GPa on the target material. Two characteristic features of heterogeneous initiation are evident: some reaction occurs just behind the shock front causing it to grow in pressure and most of the reaction occurs well behind the leading shock creating a pressure wave that overtakes the shock causing the final transition to detonation. In this case the transition to detonation occurred just before the forth gauge station at about 11.4 mm into the target.

When the target is initially heated to a higher temperature, it becomes more sensitive and requires a much lower dynamic loading to cause the transition to detonation to take place at about the same distance from the impact point. Figure 4 shows such a case where the target was initially heated to the temperature of 250˚C and then shock loaded to pressure of 3 GPa. Transition to detonation occurred at around the same 11 mm depth into the target. The shock wave steadily rose in pressure indicating that some reaction took place close to the shock front. The reasons for heated material being more sensitive to shock are: thermal expansion which leads to lower density and the creation of more voids within the material and thus more hot spots to initiate reaction and the faster growth of these hot spots into the surrounding pre-heated particles.

By confining the reactive material in a stainless steel casing one can somewhat suppress the thermal expansion and bring the shock sensitivity down. This case is illustrated in Fig. 5, where the same LX-17 was confined by steel and heated to the same temperature of 250˚C. With an impact pressure of 80 GPa, the transition to detonation took place around 12 mm into the target. Shock sensitivity of LX-17 for various initial pressures is illustrated in Fig. 6 on a so-called "Pop Plot", which displays the dependence of the distance to detonation on the initial impact pressure. On this plot one can easily compare the relative sensitivity of LX-17 at various temperatures and confinement to a more sensitive explosive HMX-based PBX 9404 at ambient conditions. On a log-log plot most of these sensitivities appear to fall on a straight line. The closer the line is to the origin of the plot the more sensitive is the material.

Similar experiments were performed on the more sensitive HMX based plastic bonded explosive LX-04, containing 85-weight % HMX and 15-weight % Viton binder at ambient room temperature and at temperatures of 150˚C and 170˚C. These are illustrated in Figures 7, 8 and 9. They all show initially a steady shock wave and then, after the reaction becomes significant, a strong growth in pressure just before the transition to detonation. Again, if LX-04 is confined in a heavy stainless steel casing, the transition to detonation is suppressed and its sensitivity is somewhat lower than that of the unconfined heated LX-04 but still higher than ambient LX-04.

When the explosive was heated to an even higher temperature (190˚C) and held at temperature for some time, the HMX underwent a solid-solid phase transition from the initial β phase to a more sensitive δ phase. The phase change was evident from the temperature traces recorded by thermocouples, which were placed into the gauge packages together with the pressure gauges. These temperature traces are shown in Fig. 10, where phase transition can easily be observed to start at about 177˚C and last for more than 20 minutes. Unfortunately, due to the severity of the environment, the pressure records are quite noisy and will not be shown here. However, the pertinent information for each experiment was retrieved from these records by looking at each trace separately.

The relative shock sensitivity of LX-04 at various initial temperatures is illustrated on the "Pop Plot" in Fig. 11.

Equation of State Analysis

Since any heated material and in particular those exhibiting energetic behavior experience significant changes in density and appear to be different at various initial temperatures one must also determine their new equation of state in the form of a new shock velocity- particle velocity (U_s-u_p) relationship. This analysis is done by using the well-known impedance matching technique and is illustrated in Fig. 12 for the case of LX-04 heated to the temperature of 150˚C.

Assuming that the EOS relations of the impactor at room temperature are very well known, one can plot the adiabat of the flyer plate originating at the flyer velocity. Experimental measurement of the initial pressure from several experiments will result in the adiabat of the new target material. Measured shock velocities between the first two or more gauge stations from the same experiments allows one to draw a line through the experimental points and determine the new U_s-u_p for this material.

For heated experiments one also has to know the density and U_s-u_p relationship of the heated buffer material so that a virtual flyer velocity can be applied. Usually the flyer and buffer materials are kept the same for the purpose of having a symmetrical impact. The thermal expansion coefficients of these materials are well known and are very small. Nevertheless there is a slight effect on the outcome of the analysis. Resulting values of the density and the $U_s - u_p$ constants for both LX-17 and LX-04 are listed in Table 1.

Ignition and Growth Reactive Flow Modeling

Since not all shock initiation scenarios can be experimentally tested, the Ignition and Growth reactive flow hydrodynamic computer code model of shock initiation and detonation have been developed based on the embedded gauge experiments discussed above to predict the results for such scenarios. All reactive flow models require as a minimum: two equations of state, one for the unreacted explosive and one for its reaction products; a reaction rate law for the conversion of explosive to products; and a mixture rule to calculate partially reacted states in which both explosive and products are present. The Ignition and Growth reactive flow model (10) uses two Jones-Wilkins-Lee (JWL) equations of state, one for the unreacted explosive and another one for the reaction products, in the temperature dependent form:

$$p = A\, e^{-R_1 V} + B\, e^{-R_2 V} + \omega C_V T/V \qquad (1)$$

where p is pressure in Megabars, V is relative volume, T is temperature, ω is the Gruneisen coefficient, C_V is the average heat capacity, and A, B, R_1 and R_2 are constants. The unreacted explosive equation of state is fitted to the available shock Hugoniot data, and the reaction product equation of state is fitted to cylinder test and other metal acceleration data. At the high pressures involved in shock initiation and detonation of solid and liquid explosives, the pressures of the two phases must be equilibrated, because interactions between the hot gases and the explosive molecules occur on nanosecond time scales depending on the sound velocities of the components. Various assumptions have been made about the temperatures in the explosive mixture, because heat transfer from the hot products to the cooler explosive is slower than the pressure equilibration process. In the Ignition and Growth model, the temperatures of the unreacted explosive and its reaction products are equilibrated. Temperature equilibration is used, because heat transfer becomes increasingly efficient as the reacting "hot spots" grow and consume more explosive particles at the high pressures and temperatures associated with detonation. Fine enough zoning must be used in all reactive flow calculations so that the results have converged to answers that do not change with even finer zoning. Generally this requires a resolution of at least 10 zones in the detonation reaction zone. The insensitive solid explosive LX-17 has an experimentally measured reaction zone length of approximately three mm (11) so using 10 zones per mm spreads the reaction over 30 zones. Shock initiation occurs over a greater thickness than detonation so using 10 zones per mm results in converged shock initiation calculations.

The Ignition and Growth reaction rate equation is given by:

$$dF/dt = I(1-F)^b(\rho/\rho_o-1-a)^x + G_1(1-F)^cF^dp^y + G_2(1-F)^eF^gp^z \quad (2)$$
$$0<F<F_{igmax} \qquad 0<F<F_{G1max} \qquad F_{G2min}<F<1$$

where F is the fraction reacted, t is time in μs, ρ is the current density in g/cm^3, ρ_o is the initial density, p is pressure in Mbars, and I, G_1, G_2, a, b, c, d, e, g, x, y, z, F_{igmax}, F_{G1max}, and F_{G2min} are constants. This three-term reaction rate law represents the three stages of reaction generally observed during shock initiation and detonation of pressed solid explosives (10). The first stage of reaction is the formation and ignition of "hot spots" caused by various possible mechanisms (void collapse, viscous flow, friction, shear, etc.) as the initial shock or compression wave interacts with the unreacted explosive molecules. Generally the fraction of solid explosive heated during shock compression is approximately equal to the original void volume. For shock initiation modeling, the second term in Eq. (2) then describes the relatively slow process of the inward and/or outward growth of the isolated "hot spots" in a deflagration-type process. The third term represents the rapid completion of reaction as the "hot spots" coalesce at high pressures and temperatures, resulting in transition from shock induced reaction to detonation.

For detonation modeling, the first term again reacts a quantity of explosive less than or equal to the void volume after the explosive is compressed to the unreacted von Neumann spike state. The second term in Eq. (2) models the fast decomposition of the solid into stable reaction product gases (CO_2, H_2O, N_2, CO, etc.). The third term describes the relatively slow diffusion limited formation of solid carbon (amorphous, diamond, or graphite) as chemical and thermodynamic equilibrium at the C-J state is approached. These reaction zone stages have been observed experimentally using embedded particle velocity and pressure gauges and laser interferometry (11 – 13).

The Ignition and Growth reactive flow model has been applied to a great deal of experimental shock initiation and detonation data using several one-, two-, and three-dimensional hydrodynamic codes. In shock initiation applications, it has successfully calculated embedded gauge, run distance to detonation, short pulse duration, multiple shock, reflected shock, ramp wave compression, and divergent flow experiments on several high explosives at various initial temperatures (heating plus shock scenarios), densities, and degrees of damage (impact plus shock scenarios) (14 – 18).

For LX-17, as discussed in the Experimental section, the shock sensitivity of unconfined charges increases greatly from 25˚C to 250˚C, but this increase can be partially overcome using heavy steel confinement. In addition to the manganin pressure gauges discussed in the Experimental section, embedded particle velocity gauges have also been developed to measure shock initiation in heterogeneous solid explosives (5,15). Figure 13 shows ten experimental and calculated particle velocity histories for the shock initiation of an ambient temperature LX-17 target impacted by a Kel-F flying plate at 2.951 km/s (15). Each particle velocity gauge is about 0.85 mm deeper than the previous one. The initial shock pressure of 14.96 GPa increases at each gauge position, but the main growth of reaction is behind the shock wave front. When the growing pressure wave overtakes the initial shock, transition to detonation occurs, as shown on the last four gauges of Fig. 13. Ignition and Growth parameters calibrated to embedded pressure gauge measurements are used to calculate the growth to detonation measured by the embedded particle velocity gauges in Fig. 13. Therefore the embedded pressure and particle velocity gauge techniques yield equivalent shock initiation data.

Figures 14 and 15 show embedded pressure gauge comparisons for 250˚C LX-17 charges impacted by aluminum flyers at 0.836 km/s and 1.11 km/s unconfined (7) and with steel confinement (9), respectively. The increased sensitivity of unconfined LX-17 at 250˚C was calculated using a lower initial density (due to the large thermal expansion of unconfined LX-17) and thus more ignition in the first term of the reaction rate equation (2) plus a larger growth of reaction coefficient G_1 in the second term of Eq. (2). Since the heavy steel confinement prohibits the growth LX-17 during heating to 250˚C, a higher density causing less ignition together with the same growth coefficient G_1 was used to calculate the confined LX-17 charge. Pure ultrafine particle size TATB has also been studied with embedded manganin gauges and reactive flow modeling at 250˚C (16).

Embedded pressure gauges and the Ignition and Growth model are also used to study preheated, shocked explosives based on the more sensitive explosive HMX. Figure 16 contains four pressure histories in 190˚C LX-04 (85% HMX and 15% Viton binder) impacted by an aluminum flyer plate at 0.92 km/s and the corresponding Ignition and Growth calculations (17). This temperature is sufficient to cause the conversion of beta HMX to delta HMX before shock impact occurs. The LX-04 containing delta HMX is more sensitive than LX-04 containing beta HMX at temperatures of 25˚C, 150˚C, and 170˚C (18). Embedded pressure gauge histories and Ignition and Growth simulations for the shock initiation of LX-04 at 25˚C (8,9), 150˚C (18) and 170˚C (8,9) are shown in Figs. 17, 18, and 19, respectively. The close agreement between the 150˚C and 170˚C LX-04 records in Figs. 20 and 21 implies that the beta to delta phase transition had not occurred at 170˚C during the time that the charges was held at temperature before impact. The growth of reaction coefficient G_1 in Eq. (2) was increased from 100 at 25˚C to 210 for 150˚C and 170˚C to 300 for 190˚C to match the experimental pressure histories (17).

The use of different equations of state and reaction rate parameters in the Ignition and Growth model for an explosive at various initial temperatures works well. However, all chemical reaction rates depend upon the local temperature of the molecules reacting at that time. Thus eventually a totally temperature dependent reactive flow model will be required. A great deal of experimental time resolved temperature data on reacting “hot spots” and the surrounding heated explosive particles will be needed to calibrate such a model. Assuming that this experimental temperature data does become available, the next generation of hydrodynamic computer code reactive flow models for simulating shock initiation and detonation in one-, two-, and three-dimensions will be based entirely on temperature dependent Arrhenius rate laws, replacing current compression and pressure dependent rate laws (10). A mesoscale model has been formulated in which individual particles of a solid explosive plus their binders and voids are meshed, shocked, and either react or fail to react using Arrhenius kinetics (19). Using descriptions of individual particles is impractical for larger scale simulations even with today’s large parallel computers, so a continuum Statistical Hot Spot reactive flow model is currently being developed in the ALE3D hydrodynamic computer code (20). In this model, realistic numbers of hot spots of various sizes, shapes, and temperatures based on the original void volume, particle size distribution and temperature of the solid explosive are assumed to be created as the initiating shock front compresses the explosive particles. The hot spots then either react and grow into the surrounding explosive or fail to react and die out based on multi-step Arrhenius kinetics rates (21). The Statistical Hot Spot reactive flow model has accurately simulated for the first time the experimentally well-

known phenomenon of "shock desensitization," in which a detonation wave fails to propagate in a pre-compressed solid explosive (20,22). The coalescence of growing hot spots at high pressures and temperatures, the creation of additional surface area available to the reacting sites as the pressure rises, and the rapid transition to detonation are three of the most challenging current problems under investigation in hydrodynamic reactive flow modeling of shock initiation and detonation in heterogeneous solid explosives.

ACKLOWLEDGEMENTS

This work was performed under the auspices of the United States Department of Energy by the Lawrence Livermore National Laboratory under Contract No. W-7405-ENG-48.

This work was performed under the auspices of the U.S. Department of Energy by University of California, Lawrence Livermore National Laboratory under contract No. W-7405-Eng-48.

REFERENCES

1. J. H. S. Lee, "Initiation of Gaseous Detonation," *Ann. Rev. Phys. Chem.* **28**, 75 – 104 (1977).
2. A. N. Dremin, "Toward Detonation Theory," Springer-Verlag, New York, 1999, Chapter 2.
3. F. P. Bowden and Y. D. Yoffe, "Initiation and Growth of Explosion in Liquids and Solids," Cambridge University Press, 1985.
4. P. A. Urtiew, J. W. Forbes, C. M. Tarver, and F. Garcia, "Calibration of Manganin Pressure Gauges at 250˚C, *Shock Compression of Condensed Matter-1999,* M. D. Furnish, L. C. Chhabildas, and R. S. Hixon, eds., AIP Conference Proc. 515, 2000, pp. 1019 – 1022.
5. P. A. Urtiew, L. M. Erickson, B. Hayes, and N. L. Parker, "Pressure and Particle Velocity Measurements in Solids Subjected to Dynamic Loading," *Combustion, Explosion and Shock Waves* **22**, 597 – 614 (1986).
6. P. A. Urtiew, T. M. Cook, J. L. Maienschein, and C. M. Tarver, "Shock Sensitivity of IHE at Elevated Temperatures," *Tenth International Detonation Symposium,* ONR 33395-12, Boston, MA, 1993, pp. 139 - 147.
7. P. A. Urtiew, C. M. Tarver, J. L. Maienschein, and W. C. Tao, "Effects of Confinement and Thermal Cycling on the Shock Initiation of LX-17," *Combustion and Flame* **105**, 43 – 53 (1996).
8. P. A. Urtiew, C. M. Tarver, J. W. Forbes, and F. Garcia, "Shock Sensitivity of LX-04 at Elevated Temperatures," *Shock Compression of Condensed Matter-1997,* S. C. Schmidt, D. P. Dandekar, and J. W. Forbes, eds., AIP Press, 2000, p. 727 - 730.
9. J. W. Forbes, C. M. Tarver, P. A. Urtiew, and F. Garcia, "The Effects of Confinement and Temperature on the Shock Sensitivity of Solid Explosives," *Eleventh International Detonation Symposium*, ONR 33300-5, Snowmass, CO, 1998, pp.147 - 152.
10. C. M. Tarver, J. O. Hallquist, and L. M. Erickson, "Modeling Short Pulse Duration Shock Initiation of Solid Explosives," *Eighth Symposium (International) on Detonation,* Naval Surface Weapons Center NSWC MP86-194, Albuquerque, NM, 1985, pp. 951 - 961.
11. C. M. Tarver, J. W. Kury, and R. D. Breithaupt, "Detonation Waves in Triaminotrinitrobenzene," *Journal of Applied Physics* **82**, 3771 - 3782 (1997).
12. C. M. Tarver, R. D. Breithaupt, and J. W. Kury, "Detonation waves in Pentaerythritol Tetranitrate," *Journal of Applied Physics* **81**, 7193 - 7202 (1997).
13. C. M. Tarver, W. C. Tao, and C. G. Lee, "Sideways Plate Push Test for Detonating Solid Explosives," *Propellants, Explosives, Pyrotechnics* **21**, 238 - 246 (1996).
14. C. M. Tarver, J. W. Forbes, F. Garcia, and P. A. Urtiew, "Manganin Gauge and Reactive Flow Modeling Study of the Shock Initiation of PBX 9501," *Shock Compression of Condensed Matter-2001*, M. D. Furnish, N. N. Thadhani, and Y. Horie, eds., AIP Press, 2002, p. 1043 - 1046.
15. R. L. Gustavsen, S. A. Sheffield, R. R. Alcon, J. W. Forbes, C. M. Tarver, and F. Garcia, "Embedded Electromagnetic Gauge measurements and Modeling of Shock Initiation in the TATB Explosives PBX 9502 and LX-17," *Shock Compression of*

Condensed Matter-2001, M. D. Furnish, N. N. Thadhani, and Y. Horie, eds., AIP Press, 2002, p. 1019 - 1022.
16. P. A. Urtiew, J. W. Forbes, F. Garcia, and C. M. Tarver, "Shock Initiation of UF-TATB at 250˚C," *Shock Compression of Condensed Matter-2001*, M. D. Furnish, N. N. Thadhani, and Y. Horie, eds., AIP Press, 2002, p. 1039 – 1042.
17. P. A. Urtiew, J. W. Forbes, C. M. Tarver, K. S. Vandersall, F. Garcia, D. W. Greenwood, P. C. Hsu, and J. L. Maienschein, "Shock Sensitivity of LX-04 Containing Delta Phase HMX at Elevated Temperatures," *Shock Compression of Condensed Matter - 2003*, M. D. Furnish, ed., AIP Press, 2004, p. 1053 - 1056.
18. C. M. Tarver, J. W. Forbes, P. A. Urtiew, and F. Garcia, "Shock Sensitivity of LX-04 at 150˚C," *Shock Compression of Condensed Matter-1999,* M. D. Furnish, L. C. Chhabildas, and R. S. Hixon, eds., AIP Conference Proc. 515, 2000, pp. 891 - 894.
19. J. E. Reaugh, "Grain-Scale Dynamics in Explosives," LLNL Report UCID-150388, Sept. 2001.
20. A. L. Nichols and C. M. Tarver, "A Statistical Hot Spot Reactive Flow Model for Shock Initiation and Detonation of Solid High Explosives," *Twelfth International Detonation Symposium*, San Diego, CA, August 2002, in press.
21. C. M. Tarver, S. K. Chidester, and A. L. Nichols, "Critical Conditions for Impact- and Shock-Induced Hot Spots in Solid Explosives," Journal of Physical Chemistry **100**, 5794 -5799 (1997).
22. A. L. Nichols, C. M. Tarver, and E. M. McGuire, "ALE3D Statistical Hot Spot Model results for LX-17," *Shock Compression of Condensed Matter - 2003*, M. D. Furnish, ed., AIP Press, 2004, pp. 397- 400.

Table 1. Density and $U_s - u_p$ constants for LX-04 and LX-17 at Various Initial Temperatures ($U_s = c + su_p$)

Explosive	Temperature (˚C)	Density (g/cm^3)	c(km/s)	s
LX-17	25	1.89	1.67	2.86
LX-17	250	1.696	1.26	2.5
LX-04	25	1.85	2.28	2.45
LX-04	150	1.784	1.12	3.9
LX-04	170	1.774	1.0	3.36
LX-04	190	1.633	1.15	1.6

FIGURE CAPTIONS

Figure 1. Streak photograph of gaseous (a) – initiation, and (b) - onset of detonation process in a stoichiometric Hydrogen – Oxygen mixture initially at low pressure.

Figure 2. Experimental set-up used to study initiation process in heterogeneous solid explosives. It depicts a moment as the projectile with an impactor leaves the gun barrel just before striking the target assembly. The target assembly is fitted with manganin pressure gauges and thermocouples at various depth of the target and with pins ahead of the target to measure the impact velocity and the tilt of the impact.

Figure 3. Pressure histories in ambient LX-17 impacted by an aluminum flyer at 1.68 km/s.

Figure 4. Pressure histories in a hot 250 C LX-17 impacted by an aluminum flyer at 0.81 km/s.

Figure 5. Pressure histories in a steel confined hot 250 C LX-17 impacted by a steel flyer at 1.16 km/s.

Figure 6. "Pop Plot" of LX-17 at various initial temperatures demonstrating its sensitivity to impact pressure.

Figure 7. Pressure histories of ambient LX-04 impacted by a steel flyer through a Teflon buffer at 0.509 km/s.

Figure 8. Pressure histories in hot 150 C LX-04 impacted by an aluminum flyer at 0.701 km/s.

Figure 9. Pressure histories in hot 170 C LX-04 impacted by an aluminum flyer at 0.515 km/s.

Figure 10. Thermal traces at various depth of the target during the heating process to the desired temperature of 190 C. The figure shows a distinct evidence of the β to δ phase transition process in HMX occurring above 175 C.

Figure 11. "Pop Plot" for LX-04 at various initial temperatures demonstrating its sensitivity to impact pressure.

Figure 12. Analysis of experimental data to determine new Shock velocity – Particle velocity relationship for LX-04 heated to 150 C.

Figure 13. Particle velocity histories for LX-17 impacted by a Kel-F flyer at 2.951 km/s

Figure 14. Experimental and calculated pressure histories in unconfined 250˚C LX-17 impacted by an aluminum flyer at 0.836 km/s

Figure 15. Pressure histories for steel confined 250˚C LX-17 impacted by a steel flyer at 1.11 km/s

Figure 16. Experimental (solid) and calculated (dashed) pressure profiles in 190˚C LX-04 impacted by an aluminum flyer at 0.92 km/s

Figure 17. Experimental and calculated pressure histories for 25˚C LX-04 impacted by a Teflon flyer at 0.956 km/s

Figure 18. Experimental and calculated pressure histories for 150˚C LX-04 impacted by an aluminum flyer at 0.594 km/s

Figure 19. Experimental and calculated pressure histories for 170˚C LX-04 impacted by an aluminum flyer at 0.515 km/s

Figures

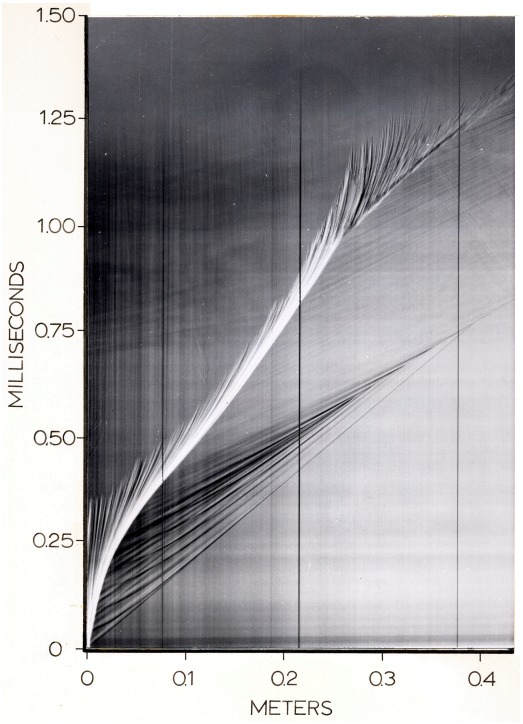

Figure1a

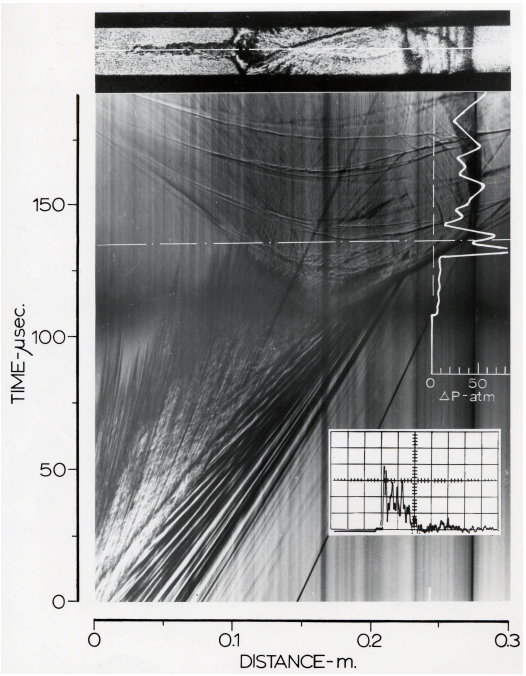

Figure 1b

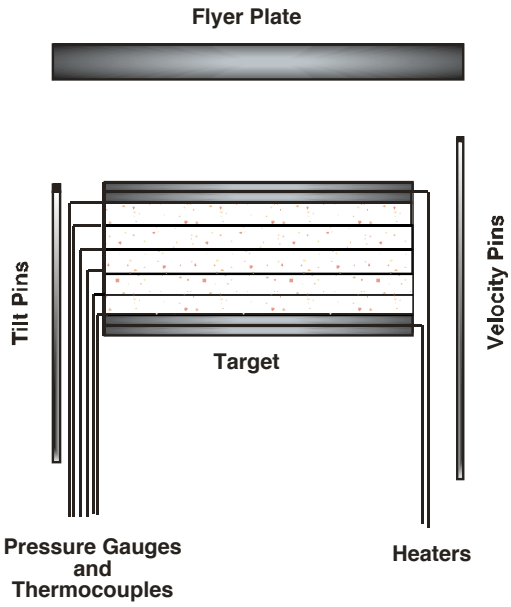

Figure 2

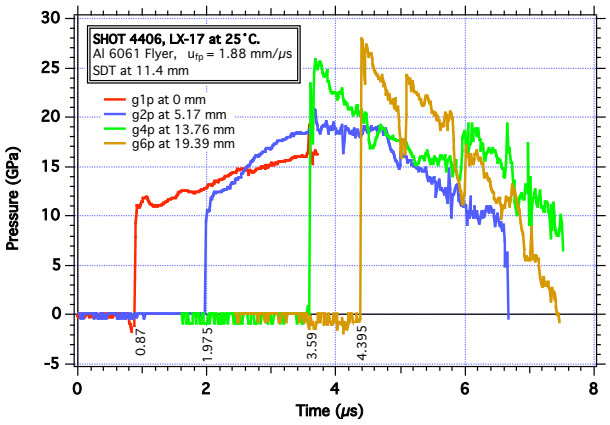

Figure 3

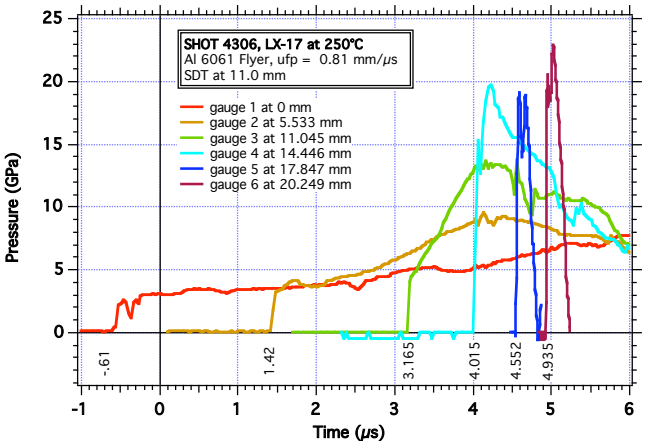

Figure 4

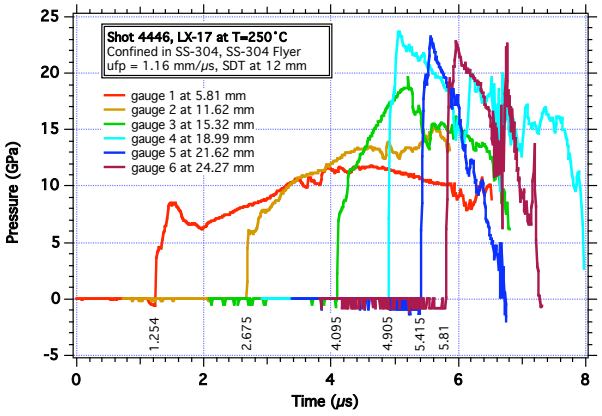

Figure 5

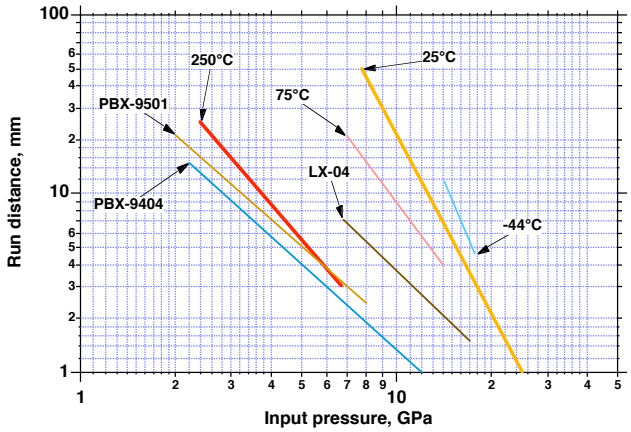

Figure 6

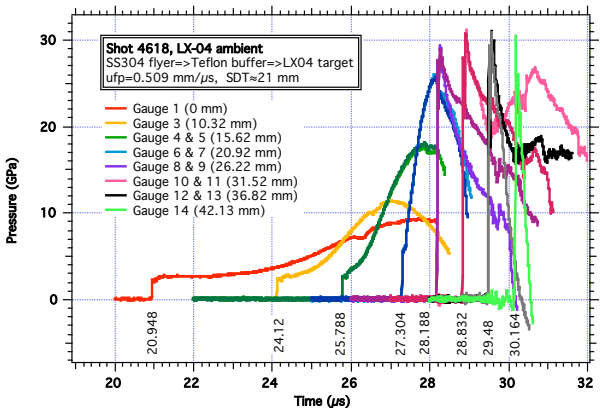

Figure 7

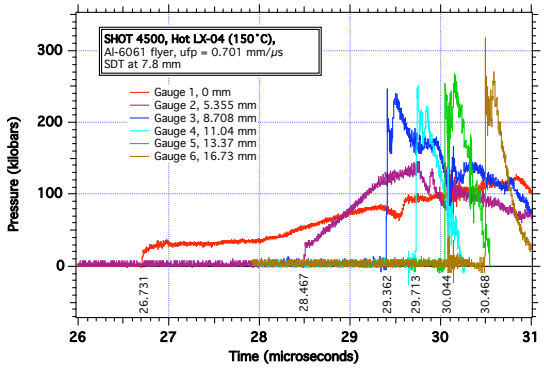

Figure 8

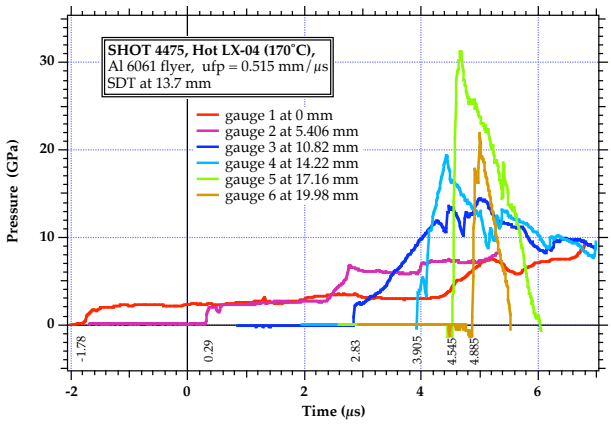

Figure 9

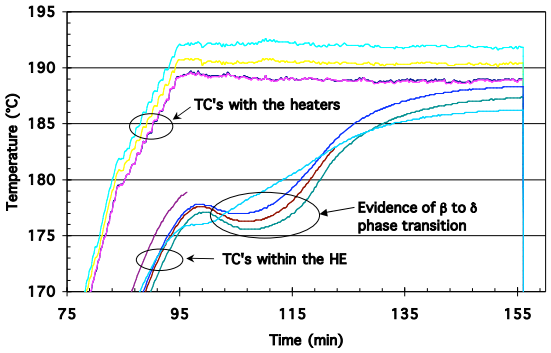

Figure 10

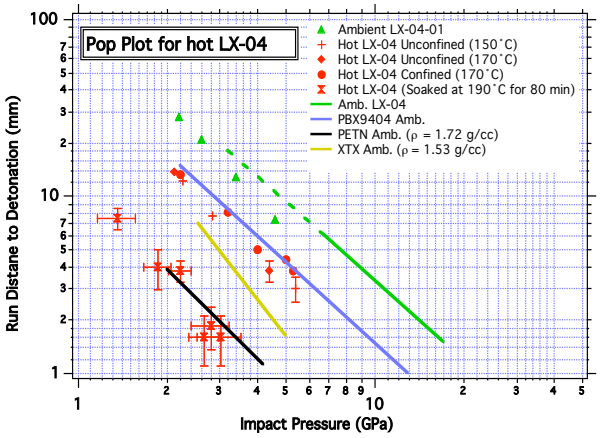

Figure 11

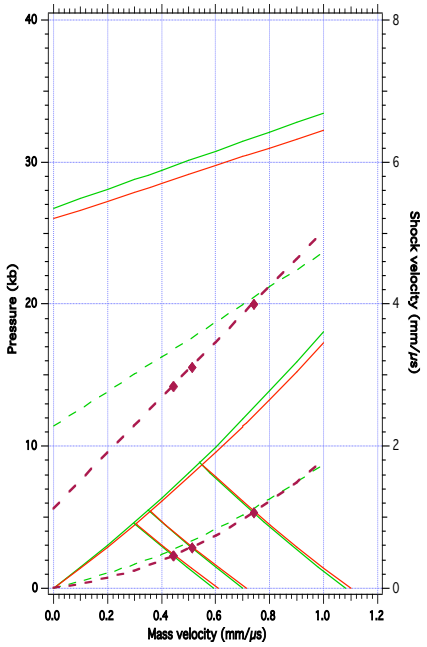

Figure 12

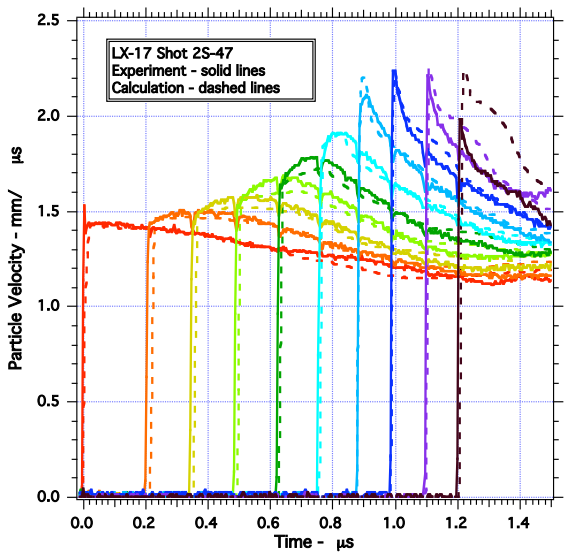

Figure 13

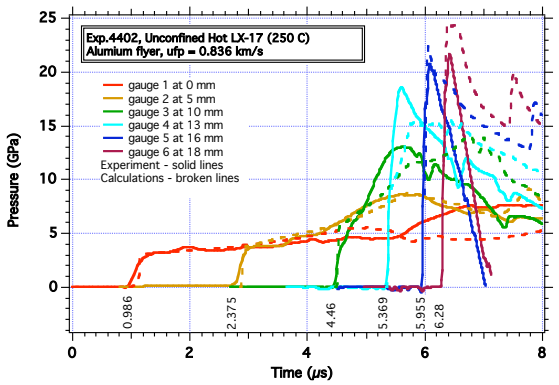

Figure 14

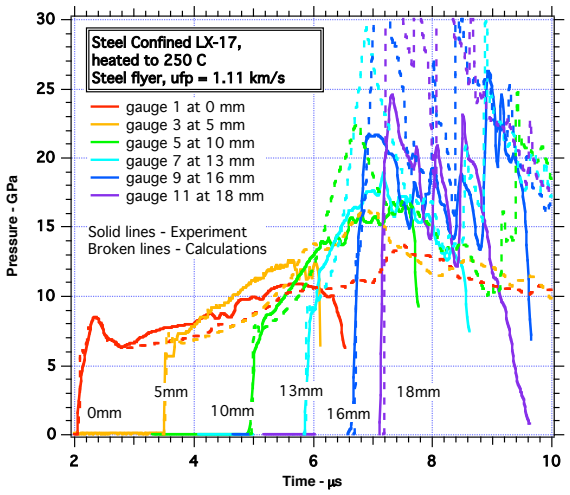

Figure 15

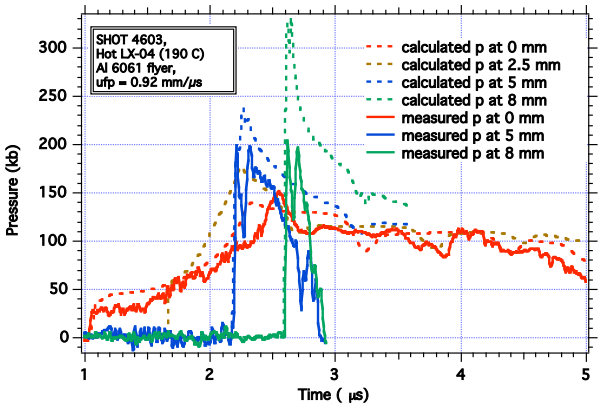

Figure 16

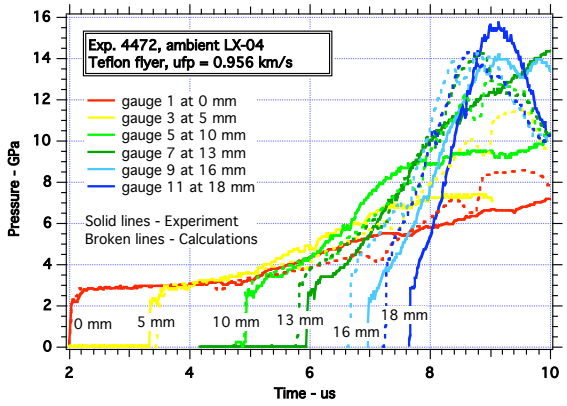

Figure 17

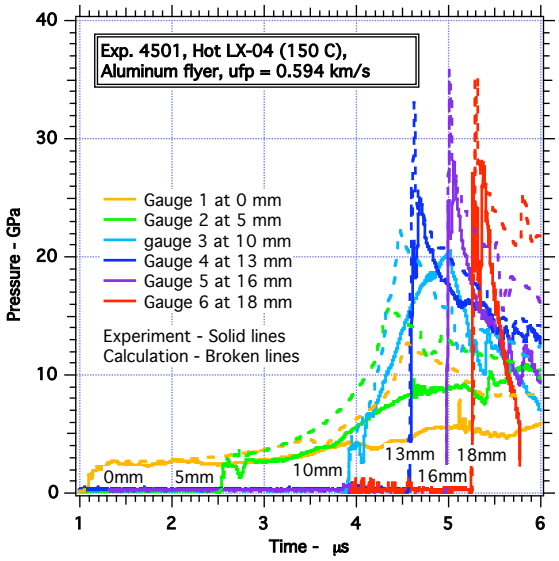

Figure 18

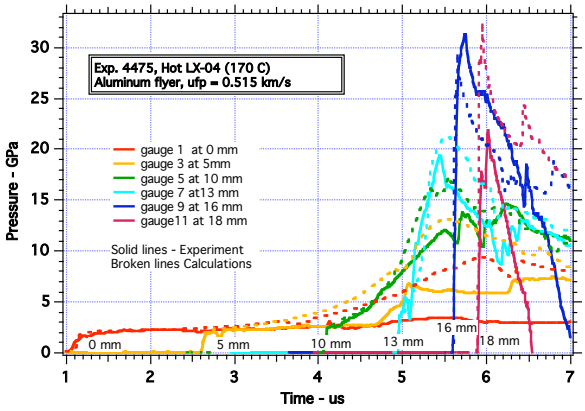

Figure 19